TERRASAR-X HIGH RESOLUTION SPOTLIGHT PERSISTENT SCATTERER INTERFEROMETRY

Stefan Gernhardt[(1)], Nico Adam[(2)], Michael Eineder[(2)], Richard Bamler[(1,2)]

[(1)]Remote Sensing Technology, Technische Universität München, Arcisstr. 21, 80333 München, Germany
Stefan.Gernhardt@bv.tu-muenchen.de
[(2)]Remote Sensing Technology Institute, German Aerospace Center (DLR), 82234 Wessling-Oberpfaffenhofen, Germany
{Nico.Adam | Michael.Eineder | Richard.Bamler}@dlr.de

ABSTRACT

The new class of meter-resolution spaceborne SAR systems (TerraSAR-X and COSMO-Skymed) offers a tremendous improvement in interferometric monitoring of urban areas and man-made infrastructure. The high resolution fits well to the inherent scale of buildings (floor height, distance of windows, etc.). In particular, Persistent Scatterer Interferometry (PSI) benefits substantially from this new data quality. Several tens or hundreds of persistent scatterers (PS) per building can for the first time be exploited for geodetic analysis from space. Many small constructive elements of buildings, like edges in facades originating from notches of windows and similar structures act as stable scatterers and thus are detected as PS at a wavelength of 3.1cm. The large amount of PS on single objects establishes the opportunity to monitor e.g. structural stress or seasonal deformation of certain objects of interest.

1. INTRODUCTION

Since the introduction of Persistent Scatterer Interferometry in the late 1990s [7], deformation regimes on large as well as small scales have been investigated, reporting an accuracy of motion up to 1mm/y [3][8]. Analyses have been based on medium resolution SAR data, available from ERS and ENVISAT satellites. Now, the era of very high resolution (VHR) radar data has begun with the launch of TerraSAR-X and COSMO-Skymed, and, from this change in resolution, new potentials arise for PSI. First results have been presented in [1] and [2].
In this investigation we will show how the number of PSs depends on resolution**,** incidence angle, and polarization. To this end the area of the Berlin inner city has been acquired by TerraSAR-X in high resolution spotlight mode at 300 MHz (slant range resolution = 0.6 m, azimuth resolution = 1.1 m) using beams with 3 different elevation angles in ascending and in descending, leading to six stacks for PSI evaluation. The comparison will be carried out on several regions in order to show the impact of the corresponding parameters on the density of PS for different characteristics of buildings, as they are typical for European cities.

The deformation estimates of the six stacks of Berlin show a very interesting pattern at the central railway station. It turns out that a linear deformation model insufficiently describes the movement at this location and consequently a more complex model has to be introduced. The results of PS deformation estimation using a seasonal sinusoidal model comprise several very interesting patterns, which will be presented in this study. Periodic deformation in vertical as well as horizontal directions of the building parts and the rail tracks follow a pattern of thermal expansion of steel. The amplitudes are shown to be consistent with temperature records for the given area. Especially the unique constellation of six different stacks covering the same region facilitates the interpretation of deformation. Vertical and horizontal contributions can be separated, which could be validated by constructional conditions of the building and the rail tracks.
Besides the deformation parameters a height update relative to the used digital elevation model is estimated, using the PSI processing software PSI-GENESIS of DLR. To this end the exact 3D positions of the PS are retrieved both in the azimuth-range-elevation system and, after geocoding, in x, y and z UTM co-ordinates. After correct calibration to the elevation angle of the reference point, all geolocation errors in range and azimuth should be less than 0.5 meters for TerarSAR-X. The precision of the localization depends amongst others on the number of acquisitions, the baseline distribution and the signal to noise ratio and can be assessed in advance for the given stack and parameters of acquisition. In this paper the expected precision will be compared to the one obtained from PSI stacking by evaluating the distribution of scatterers from rows of windows in facades of buildings which accumulate in a line. This constellation of PS could be observed at different buildings in the data and serve as a basis for this investigation.

2. DATA PROCESSING

The area of interest in this investigation has been defined to the inner city of Berlin, Germany, centered on the main railroad station. Altogether, six different stacks of data takes (all in VV polarisation mode) have

Proc. 'Fringe 2009 Workshop', Frascati, Italy,
30 November – 4 December 2009 (ESA SP-677, March 2010)

been acquired, covering approximately one year starting in February 2008. Table 1 shows the number of images in each stack which ranges from 16 up to 22 depending on acquisition conflicts with other users or customers. These six stacks can be separated in two groups: one ascending and one descending track, each containing three different beams, which imply certain incidence angles for data capture. The available angles are 30°, 42° and 51° for the ascending beam numbers 28, 57 and 85 and 36°, 47° and 55° for the descending beam numbers 42, 70 and 99 respectively. They represent appropriately the incidence angles of the acquisitions at the centre of the dataset. Due to these different viewing directions the covered area ranges from 33 km^2 to 51 km^2, whereas steep angles produce larger coverage than flat ones. The given datasets of six groups represent the input for the following processing in order to obtain PS positions in each set of images. All data stacks have been processed using PSI-GENESIS of DLR, which has been adapted for spotlight mode data [6].

Table 1: acquisition parameters: incidence angle, track type, area and number of data sets in each stack

Beam no.	Inc. Angle	Track Type	Area [km^2]	No. of Data
28	30°	Ascending	50.8	22
57	42°	Ascending	40.7	15
85	51°	Ascending	33.0	21
42	36°	Descending	42.9	20
70	47°	Descending	36.8	21
99	55°	Descending	34.2	22

3. PERSISTENT SCATTERER DENSITIES

At the moment, no comparable stack of high resolution spotlight data in HH polarisation is available for the area under investigation. Nevertheless, a first analysis has been carried out on a small subset of data with equal number of datasets in HH as well as VV polarization to assess the differences in PS densities concerning polarization. For the selection of the PS, a threshold on signal-to-clutter ratio has been used [4]. In figure 1 three examples of local densities are shown, including different alignments between the city structure and the sensor orientation. In area 1 building facades are aligned perpendicularly to the sensor for ascending tracks. In the second area the distribution of building walls facing the sensor is approximately equally distributed for both track types, whereas in area 3 there is no main orientation. The density assessments of the selected regions within the given scenes show, that HH datasets hold an overall 5-10% increase in number of PSs per square kilometer, locally even up to 20%. An example is presented in figure 2, where the facade of a high rise building shows many PSs in HH data and just a few at the side in VV polarization. But in general there is no strong preference for a certain polarization. Accordingly, PSI processing can be carried out successfully using any of both polarizations.
The influence of geometrical parameters on the number of PS can be extracted from the comparison of the different areas (see Fig. 1). Starting from area 1, PS densities decrease significantly if moving to areas with less (area 2) or even no (area 3) alignment of building facades perpendicular to viewing direction of the satellite. Therefore the highest number of PS can be extracted from facades that face towards the sensor. In addition, comparison of area 2 and area 3 hold, that shadow effects result in a slight drop in number of PS, dependent on building heights and distances, if moving from mid-range to large incidence angles. Another decrease in PS densities caused by shallow incidence angles results from reduced resolution in vertical directions, and therefore influences PS retrieval on facades. The combination of decreasing effects can be seen in figure 3. Besides the loss of PS from lower floors due to shadow of the nearby buildings, some of the single rows of PS originating from different levels cannot be separated for large incidence angles.
All together, the main influence on PS densities arises

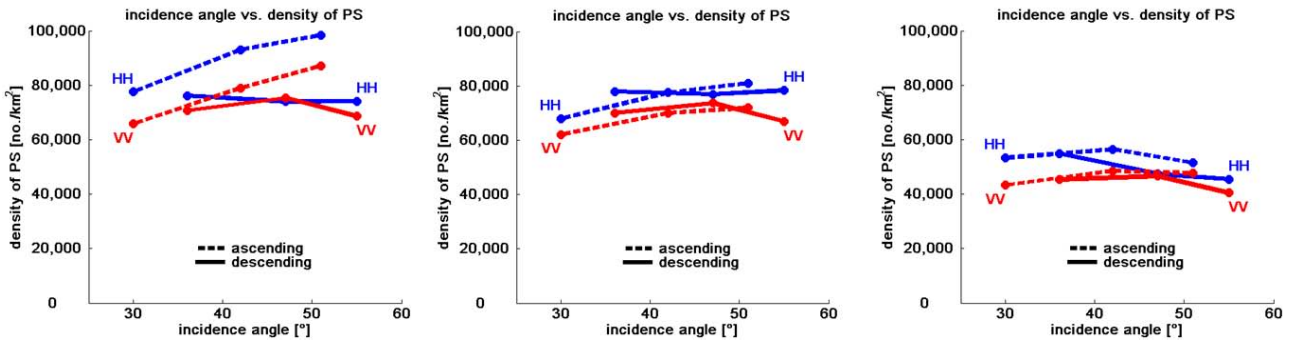

Figure 1: PS density plots with respect to increasing incidence angles for three different areas in Berlin; From left to right: area 1 (main orientation of buildings parallel to ascending tracks), area 2 (equal distribution of facades perpendicular to sensor orientation for both track types) and area 3 (no main orientation);

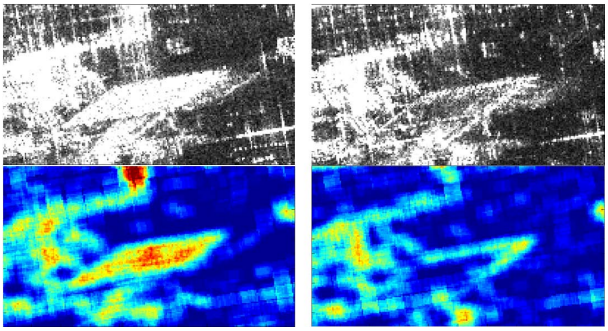

Figure 2: PS density depending on polarizations. left: HH, right: VV, upper figures: radar mean maps, lower figure: PS densities (red colors indicate high, blue colors low density)

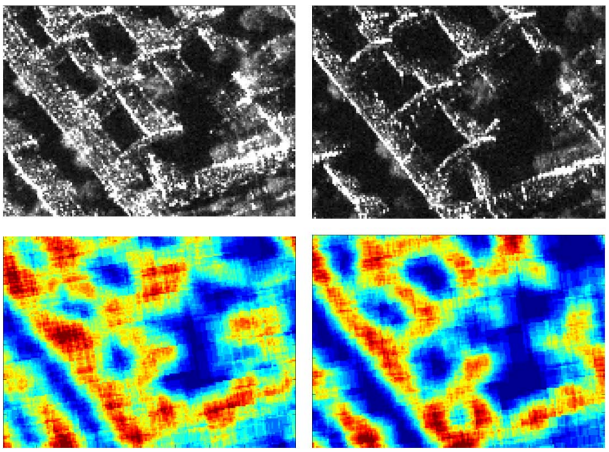

Figure 3: up: mean intensity maps, down: PS densities, red colors indicate high, blue low density; left figures: incidence angle of 42°, right figures: incidence angle of 51°; both ascending cases; with rising incidence angle PS densities drop due to loss of resolution in elevation direction and shadow areas

Figure 4: Berlin central train station

from the unique geometrical configuration given by acquisition parameters and the alignment of the objects within the scene, including orientation, distance and height.

4. DEFORMATION ASSESSMENTS

An interesting test case is the central railroad station of Berlin shown in figure 4. PSI processing of the area and a detailed analysis of several phase histories of PSs on the object finally resulted in a combination of a linear and a periodic displacement model. The period has been fixed to one year and the parameters amplitude and temporal offset of the sine function are estimated. The estimated seasonal amplitudes are color-coded visualized in figure 5, where the identified PSs are overlaid on the radar mean map. On the left hand side, the ascending case is illustrated with a viewing direction from left to right. On the right hand side, data from a descending orbit has been evaluated and the viewing direction is opposite of the previous case (right to left). In both images, blue color indicates movement towards the sensor, whereas red color denotes displacement in the opposite direction. Due to the availability of two observation directions it is possible to separate horizontal and vertical displacement: left and right of the main part of the building the halls experience a horizontal seasonal deformation, which shows up in an expansion to both sides (central part of both halls is stable; location indicated by white bar), while the central part is moving in vertical direction. Decomposing all 6 vectors of line-of-sight (LOS) deformation for a small region at the top of the central building as well as the tower shows large vertical components at both positions of 8.7 mm. Another interesting section can be found in upper right corner, where two parts of the bridge and tracks are moving towards each other in summer time. The decomposition in west-eastern and vertical directions reveal a movement of the western part of 8.8 mm to the east, while the eastern part is moving to the opposite direction showing an amplitude of 6.4 mm. Due to these movements, an expansion gap is present, which has been approved by ground truth inspection.

In this example, all deformations are correlated to thermal expansion during summer time and shrinking in winter time of the steel construction, e.g. the central part shows an amplitude of 8 mm of vertical displacement which corresponds to 16 mm total movement between winter and summer. If the deformation amplitudes of the points are analyzed versus height above ground, a linear correlation is observed. As the building is constructed from steel, the difference in temperature can be calculated which is necessary to expand steel up to 16 mm on a length of approximately 45 m (which is the height of the given structure) from

$$\Delta T = \frac{\Delta L}{kL} = \frac{0.016m}{12.2e^{-6}K^{-1}45m} = 29.1°K \qquad (1)$$

Considering the temperature history of Berlin between February 2008 and February 2009, which corresponds to the used time interval of the TerraSAR-X acquisitions, the mean differences in high and low temperature differences are 33°C and 29°C respectively. This fits the calculated temperature very well and supports the assumption of thermal expansion of the building.

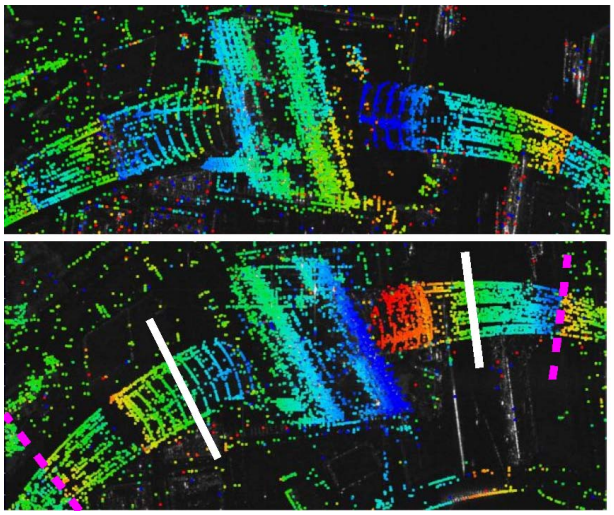

Figure 5: up: ascending track (incidence angle: 51°), viewing direction from left to right. down: descending case (incidence angle: 55°), viewing direction from right to left. Both cases: blue colors indicate movement towards the sensor, red colors indicate movement away from the sensor. White bars on right image show stable centers of horizontally expanding halls; purple dashed bar indicates construction gap for movement of rail tracks towards each other

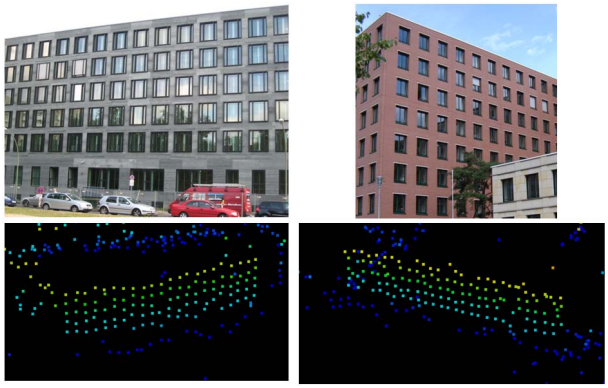

Figure 6: two examples for PS originating from lines of windows on facades; up: photographs of the objects; down: geocoded PS of both buildings showing regular pattern

5. RELATIVE PRECISION OF LOCALIZATION

Besides deformation estimates PSI delivers height updates with respect to the used DEM during processing. In the Berlin test case the final geocoded PS positions are investigated on their relative accuracy. As many PS show up on facades using high resolution spotlight data, scatterers originating from windows are evaluated, as these points are assumed to show up as regular patterns. From several buildings this assumption could be approved. Two examples are shown in figure 6, including photographs of the real world objects. For both examples a least-squares adjustment has been carried out, estimating a line from the PS with a horizontal orientation as well as a regular sampling. The two mentioned restrictions shall be fulfilled by a row of windows on buildings. After the estimation, the mean distances of all PS belonging to the line are calculated in range r, azimuth x and elevation direction s. In both cases the regular sampling is estimated to be 2.7 m, whereas the mean deviation in azimuth and range are between 6 cm and 21 cm. In contrast, the mean differences in elevation directions are 94 cm and 41 cm respectively. The worse determination by factor 2 to 5 in comparison to range/azimuth is in agreement with the expectation, as the estimates in elevation direction are dependant on the standard deviation of the baseline and number of acquisitions. According to [5], the Cramér-Rao Lower Bound (CRLB) on elevation estimates using a stack of SAR-data can be written as:

$$\sigma_{\hat{s}} = \frac{\lambda r}{4\pi\sqrt{\mathrm{NOA}}\cdot\sqrt{2\,SNR}\cdot\sigma_{Bs}} \qquad (2)$$

Using a wavelength λ = 0.031 m, a distance of r = 588 km, 22 acquisitions (NOA) of ascending stack beam 28, which shows a standard deviation of baselines of 101.6 m, and assuming a SNR of 10dB, the CRLB for the estimates in elevation is about 70 cm.

6. CONCLUSION

The investigations shown here give an insight to potentials of PSI using high resolution spotlight data. As expected, the number of PS increases dramatically if (sub-)meter resolution SAR-data is used. As polarization does not incorporate a major influence on PS densities, data of any polarization may be used successfully for PSI. Local and global variations on number of PSs in a scene may occur from geometrical parameters like building height, orientation and distances in combination to acquisition parameters. Loss of PSs due to raising incidence angles emerges mainly from shadow effects and concurrence of floors (reduced vertical resolution).

The relative accuracy of PSs has been investigated using scatterers originating from lines of windows. These points show a regular pattern after geocoding, as anticipated. The mean deviations to a horizontal line with equal spacing match the expectation of being considerable larger in elevation than in azimuth/range, as the baseline spread for TerraSAR-X is held in a tube of only 500 m diameter by mission control.

On the main object of interest – Berlin central train station – thermal expansion of the steel construction could be discovered from the correlation of the seasonal amplitudes on height of the PSs. The necessary temperatures for the expansion could be assessed by the examination of temperature histories covering the time of acquisitions. Besides the comparison of results from ascending and descending stacks, the decomposition of LOS displacement in west-eastern and vertical

directions showed the main components of displacements. The horizontal movements on the bridge eastwards to the train station hold the position of a constructional gap, proved by ground truth inspections. Of course, only movement fitting the used displacement model can be detected precisely, while the temporal sampling of 11 days at minimum depicts another limiting factor on movements. Nevertheless especially the estimation results on the train station and the tower besides it show the potential of VHR SAR-data: Single object observation and stress analysis become applicable from space, covering deformation phenomena up to sub-millimeter accuracy.

REFERENCES

[1] Adam, N., Eineder, M., Yague-Martinez, N. & Bamler, R., 2008: High Resolution Interferometric Stacking with TerraSAR-X, Proceedings of IGARSS 2008, Boston, USA

[2] Adam, N., Eineder, M., Yague-Martinez, N. & Bamler, R., 2008: TerraSAR-X High Resolution SAR-Interferometry – Proceedings of EUSAR, Friedrichshafen, Germany

[3] Adam, N., Parizzi, A., Eineder, M. & Crosetto, M., 2008: Practical Persistent Scatterer Processing Validation in the Course of the TERRAFIRMA Project. – Journal of Applied Geophysics, in print 2009.

[4] Adam, N.; Kampes, B.; Eineder, M., 2004: Development of a Scientific Permanent Scatterer System: Modifications for Mixed ERS/Envisat Time Series, Proceedings of the 2004 Envisat & ERS Symposium (ESA SP-572). 6-10 September 2004, Salzburg, Austria. Edited by H. Lacoste and L. Ouwehand. Published on CD-Rom.

[5] Bamler, R., Eineder, M., Adam, N., Zhu, X. & Gernhardt, S., 2009: Interferometric Potential of High Resolution Spaceborn SAR, Photogram-metrie Fernerkundung Geoinformation 5, in print 2009

[6] Eineder, M.; Adam, N.; Bamler, R.; Yague-Martinez, N.; Breit, H.; Spaceborne Spotlight SAR Interferometry With TerraSAR-X, Geoscience and Remote Sensing, IEEE Transactions on Volume 47, Issue 5, May 2009 Digital Object Identifier 10.1109/TGRS.2008. 2004714, Page(s):1524 – 1535.

[7] Ferretti, A., Prati, C. & Rocca, F., 2001: Permanent scatterers in SAR interferometry, IEEE Transactions on Geoscience and Remote Sensing 39 (1): 8-20

[8] Ferretti, A., Savio, G., Barzaghi, R., Borghi, A., Musazzi, S., Novali, F., Prati, C. & Rocca, F., 2007: Submillimeter Accuracy of InSAR Time Series: Experimental Validation. – IEEE Transactions on Geoscience and Remote Sensing 45 (5): 1142–1153.